Journal of Asian Earth Sciences 207 (2021) 104660

Contents lists available at ScienceDirect

Journal of Asian Earth Sciences

journal homepage: www.elsevier.com/locate/jseaes

Different accumulation mechanisms of organic matter in Cambrian sedimentary successions in the western and northeastern margins of the Tarim Basin, NW China

Qian Deng [a,b], Haozhe Wang [a,b], Zhiwei Wei [a,b], Shida Li [a,b], Haizu Zhang [c], Hu Liu [d], Oluwabamise Lekan Faboya [a,e], Bin Cheng [a], Zewen Liao [a,*]

[a] State Key Laboratory of Organic Geochemistry, Guangzhou Institute of Geochemistry, Chinese Academy of Sciences, Guangzhou 510640, China
[b] University of Chinese Academy of Sciences, Beijing 100049, China
[c] Research Institute of Petroleum Exploration and Development, PetroChina Tarim Oilfield Company, Korla 841000, China
[d] Shale Gas Evaluation and Exploitation Key Laboratory of Sichuan Province, Chengdu 610091, China
[e] Department of Chemical Sciences, Afe Babalola University, Ado-Ekiti, Ekiti-State, Nigeria

ARTICLE INFO

Keywords:
Organic matter accumulation
Stable organic/inorganic carbon isotope distribution
Lower Cambrian strata
Tarim Basin

ABSTRACT

Lower Cambrian black shales are widely distributed in the Tarim Basin, but those in the Keping area in the west have a high total organic carbon (TOC) content different from those in the Kuluketage area in the northeast of the basin. The Cambrian Yuertusi Formation in the Shiairike section (Keping) and the Xishanbulake Formation in the Yaerdangshan section (Kuluketage) are time-equivalent and can be correlated. Black shales of the Yuertusi Formation have lower $\delta^{13}C_{Ker}$ values (<−34‰) than the Xishanbulake Formations ($\delta^{13}C_{Ker}$ values > − 4‰). These values suggest that black shales in the Yuertusi Formation were dominated by benthic algae, whereas rocks in the Xishanbulake Formation contain substantial amounts of planktonic algae. Analyses of trace elements demonstrate an anoxic depositional environment, with high productivity in both the Yuertusi and Xishanbulake Formations. The enhanced productivity was promoted by upwelling fluids and hydrothermal events, leading to the enrichment of nutrient elements such as barium, cadmium, copper, phosphorus, nickel, vanadium, and zinc. More terrigenous inorganic detritus input to the Xishanbulake Formation, which led to less amounts of organic matter and degradation of planktonic algae during sedimentation, resulted in a lower TOC content than the Yuertusi Formation.

1. Introduction

Lower Cambrian black shales are widely distributed in the world. These shales have received considerable attention because they can provide major petroleum resources and contain many types of ore deposits (e.g., Lan et al., 2017; Yang et al., 2017; Li et al., 2018; Wan et al., 2018; Zhao et al., 2019). Lower Cambrian black shales in South China have been used to study the evolution of the Early Cambrian Ocean (e.g., Ishikawa et al., 2013; Wang et al., 2015; Jin et al., 2016; Han et al., 2018; Fang et al., 2019). Studies of the Lower Cambrian strata in the Tarim Basin, NW China are relatively few although the Tarim Basin is known to have well-preserved Cambrian successions, nevertheless this strata has recently drawn more and more attentions from researchers (e.g., Yao et al., 2014, 2017; Guo et al., 2017; Liu et al., 2017; C. Zhang et al., 2020; Y. Zhang et al., 2020).

The Tarim Basin is a large superimposed basin and has undergone multiple stages of tectonic movements and multiple periods of hydrocarbon generation, accumulation, and migration (Jia and Wei, 2002; He et al., 2005; Zhang et al., 2013; Li et al., 2019). It is one of the most important hydrocarbon-bearing basins in China. The Cambrian Yuertusi Formation in the Keping region, western Tarim Basin is known to contain a high total organic carbon (TOC) content up to 10% (Zhu et al., 2016). Sedimentary rocks of the Cambrian Yuertusi Formation have a high TOC content different remarkably from its equivalent Xishanbulake Formation in the northeastern margin of the basin. Besides, the Yuertusi Formation source rock thickness is much thinner than that in the Xishanbulake Formation. It has been proposed that the eastern part of the Tarim Basin developed in deeper water than the carbonate platform in

* Corresponding author.
E-mail address: liaozw@gig.ac.cn (Z. Liao).

https://doi.org/10.1016/j.jseaes.2020.104660
Received 12 July 2020; Received in revised form 10 December 2020; Accepted 22 December 2020
Available online 29 December 2020

the western part during the Cambrian period (Liu et al., 2011; Pan et al., 2015). This paleogeographic framework was linked with different source rocks in the Lower Cambrian Yuertusi and Xishanbulake Formations (Ren et al., 2018).

Discrepancies in TOC content could be caused by variations in primary productivity, redox conditions of the bottom water, terrigenous detritus input, and sedimentation rate between the western and northeastern basin, among other factors. In this study, the geochemical records, including TOC, carbon isotope compositions of carbonates ($\delta^{13}C_{Carb}$) and kerogens ($\delta^{13}C_{Ker}$), and major and trace element distributions, were systematically analyzed in the sedimentary rock samples collected from the Shiairike and Yaerdangshan sections. The objectives are to: (1) identify the differences in geochemical characteristics between the Cambrian successions from the two sections; (2) reconstruct the depositional environment of the Lower Cambrian strata in the Tarim Basin; and (3) compare the accumulation mechanisms of organic matter in Cambrian successions in the western and northeastern margins of the Tarim Basin.

2. Geologic setting and stratigraphy

The Tarim Basin in NW China covers an area of 560,000 km^2 and is tectonically surrounded by the Tianshan orogenic belt to the north, the west Kunlun orogenic belt to the southwest, and the Altun orogenic belt to the southeast (Fig. 1). The basin is divided into the Kuqa, North, Southwest, Southeast, and Tanggu depressions and the Tabei, Bachu, Tazhong, and Tadong uplifts (Fig. 1, Pan et al., 2015; Tian et al., 2018).

The Tarim Basin has a pre-Sinian crystalline basement overlain by well-developed post-Sinian sedimentary sequences. It is a typical superimposed basin, characterized by Sinian–Paleozoic marine sedimentary sequences overlain by Mesozoic–Cenozoic foreland and intracontinental sedimentary sequences (Zhang et al., 2013; Zhu et al., 2019). Most regions of the basin are occupied by desert, but outcrops of Precambrian and Paleozoic to Mesozoic rocks are scattered along its margins. For instance, in the western marginal Keping area and the northeastern marginal Kuluketage area, the Sinian–Cambrian sedimentary sequences are well exposed.

In the Shiairike section, Keping area, the Lower Cambrian Yuertusi Formation rests unconformably on the Sinian Qigebulake Formation and underlies the Lower Cambrian Xiaoerbulake Formation. The Qigebulake and Xiaoerbulake Formations are dominated by thick dolostones. The thickness of the Yuertusi Formation is about 20 m, which begins with a thin layer of cherts, followed by black shales and dolostones. Acritarchs, algae, and small shelly fossils are common found in the Yuertusi Formation (Yao et al., 2005; Dong et al., 2009).

In the Yaerdangshan section, Kuluketage area, the Xishanbulake Formation unconformably overlies on the Sinian Shuiquan Formation and underlies the Lower Cambrian Xidashan Formation. The Shuiquan Formation is comprised of dolostones. The Xishanbulake Formation is composed of siliceous mudstones and black shales, and the Xidashan Formation consists of dolostones in the lower part, black shales in the middle part, and thick-layered dolostones with interbedded black shales and limestones in the upper part. According to previous studies on the paleontology and stratigraphy, the Yuertusi and Xishanbulake Formations are time-equivalent to the Terreneuvian (Table 1and references therein).

3. Samples preparation and analytical methods

A total of 122 and 42 fresh sedimentary rock samples were collected from the Shiairike and Yaerdangshan sections, respectively. Any weathered surfaces or post-depositional veins were carefully removed. Sample pieces were pulverized (200 mesh) and then TOC, carbonate carbon and oxygen isotopes ($\delta^{13}C_{Carb}$ and $\delta^{18}O_{Carb}$), $\delta^{13}C_{Ker}$, and the major and trace elements contents were measured, with the details described in the following sections.

3.1. TOC analysis

About 80–120 mg of powdered rock was treated with a 15% HCl solution for over 24 h to ensure the complete carbonate removal. The decalcified solid residue was then washed repeatedly with deionized water until the pH value of the solution approached 7. The solid material was then dried at 60 °C before analysis. TOC analysis was conducted with an Eltra CS-800 Carbon Sulfur Determinator at the State Key Laboratory of Organic Geochemistry, Guangzhou Institute of Geochemistry, in Guangzhou, China.

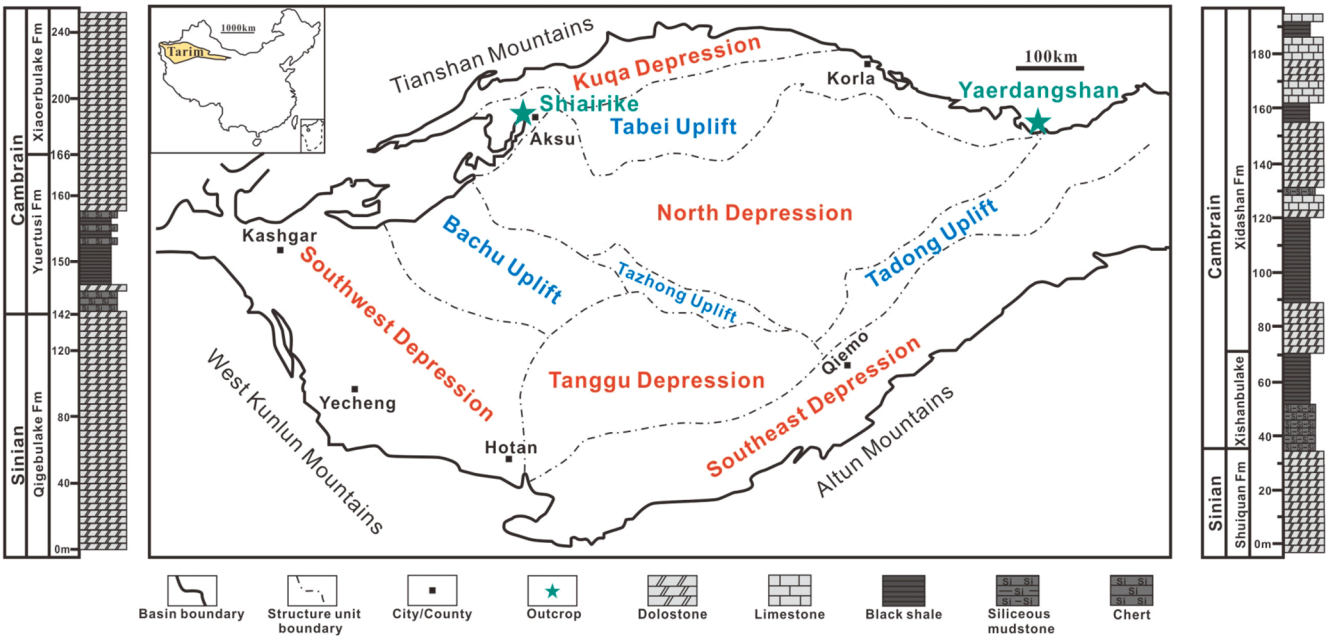

Fig. 1. The distribution of tectonic units in the Tarim Basin and the lithostratigraphic columns of the Shiairike (left) and Yaerdangshan sections (right).

Table 1
The Lower Cambrian stratigraphic correlation in the Tarim Basin (after Jia et al., 2004; Qian et al., 2009; Cohen et al., 2013; Zhang et al., 2015).

Chronostratigraphy					Numerical age (Ma)	Lithostratigraphy	
International				China		Keping-Aksu	Kuluketage
Paleozoic	Cambrian	Series 2	Stage 4	Duyunian	514	Wusonger Fm.	Xidashan Fm.
			Stage 3	Nangaoian	521	Xiaoerbulake Fm.	
		Terreneuvian	Stage 2	Meishucunian	529	Yuertusi Fm.	Xishanbulake Fm.
			Fortunian	Jinningian	541.0 ± 1.0		
Neoproterizoic	Ediacaran			Sinian		Qigebulake Fm.	Hangeerqiaoke Fm. Shuiquan Fm.

3.2. $\delta^{13}C_{Carb}$ and $\delta^{18}O_{Carb}$ analysis

Stable carbonate carbon and oxygen isotopes were determined on a Gas Bench II carbonate preparation device, which was connected to a MAT 253 mass spectrometer at the Key Laboratory of Tectonics and Petroleum Resources Ministry of Education, China University of Geosciences (Wuhan, China). Isotopic results were reported in standard δ-notion in per mil (‰) relative to the Vienna Pee Dee Belemnite standard (VPDB).

3.3. $\delta^{13}C_{Ker}$ analysis

The extraction of kerogen was performed according to the procedure proposed by Fu and Qing (1995). About 50 g of powdered rock was treated repeatedly with dilute HCl and HF to remove carbonate and silicate minerals. The residue (i.e., kerogen) was washed with deionized water until a neutral state was attained, and then the residue was dried under vacuum. The $\delta^{13}C_{Ker}$ values were measured using an elemental analyzer coupled with a conflow interface that automatically transferred carbon dioxide gas into a Finnigan Delta Plus mass spectrometer. The standard deviation of the carbon isotopic values was less than ±0.3‰.

3.4. Major and trace elements analyses

Quantification of major and trace elements was accomplished at the ALS Laboratory Group's Mineral Division, ALS Chemex, in Guangzhou, China. The oxides of major elements were measured by a Philips PW2404 X-ray fluorescence spectrometer. The relative deviation was smaller than 5%, and the relative error of the elemental concentration was smaller than 2%. For trace element content analyses, the powdered rock samples were digested using HNO_3-$HClO_4$-HF-HCl mixed acids. Organic-rich samples were firstly combusted at 750 °C to sufficiently remove the organics and then subjected to the digestion procedure. Trace element concentrations were determined by an Agilent 7700x inductively coupled plasma mass spectrometer (ICP-MS) combined with an Agilent VISTA inductively coupled plasma atomic emission spectrometer (ICP-AES). The relative deviation of the measured elemental concentration was smaller than 10%.

4. Results and discussion

4.1. Comparison of some basic geochemical results between the two sections

4.1.1. Organic matter content

For the Shiairike section, the TOC content of dolostones in the Sinian Qigebulake and Cambrian Xiaoerbulake Formations was very low (usually smaller than 0.1%). Whereas the TOC content of the Yuertusi Formation was high, ranging from 0.03% to 11.5% (average: 1.79%), indicating a distinct variation. For the Yaerdangshan section, the TOC content did not vary significantly with a range from 0.06% to 1.42% (average: 0.54%).

4.1.2. Stable carbon and oxygen isotope composition of the carbonate

For the Shiairike section, the $\delta^{18}O_{Carb}$ values of all the three studied strata ranged from −15.2‰ to −0.9‰ (average: −6.8‰). The $\delta^{13}C_{Carb}$ values for the Qigebulake, Yuertusi, and Xiaoerbulake Formations ranged from −1.46‰ to 7.26‰ (average: 3.25‰), −11.1‰ to 2.47‰ (average: ‰3.11‰), and −1.25‰ to 3.18‰ (average: 2.36‰), respectively. For the equivalent Yaerdangshan section, the $\delta^{18}O_{Carb}$ values varied from −10.7‰ to −4‰ (average: −7.8‰). The $\delta^{13}C_{Carb}$ values for the Shuiquan, Xishanbulake, and Xidashan Formations ranged from −3.75‰ to −0.77‰ (average: −2.16‰), −6.68‰ to 2.36‰ (average: −3.84‰), and −5.31‰ to −0.65‰ (average: −2.98‰), respectively. In this study, the $\delta^{18}O_{Carb}$ values of most samples exceeded −10‰, without obvious positive correlation between the $\delta^{13}C_{Carb}$ and $\delta^{18}O_{Carb}$ values (Fig. 2). This suggested that the samples were only slightly influenced by the diagenetic alteration (Derry, 2010).

The $\delta^{13}C_{Carb}$ profile of the Shiairike section (Fig. 3A) indicated a positive $\delta^{13}C_{Carb}$ value for the Qigebulake Formation, and then a gradually decreasing pattern at the upper part of the formation. At the lower part of the Yuertusi Formation, the $\delta^{13}C_{Carb}$ value decreased to a minimum of −11.1‰ and then changed to a positive value at the upper Yuertusi Formation, followed by an almost invariable positive value in the overlain Xiaoerbulake Formation. There was an obvious $\delta^{13}C_{Carb}$ excursion at the base of the Cambrian in the Shiairike section. Likewise, a negative shift was observed from −2.3‰ to −5.6‰ at the lower part of the Xishanbulake Formation in the Yaerdangshan section (Fig. 3B). Rapid climate warming and a large-scale rise in sea level may have influenced the observed $\delta^{13}C_{Carb}$ changes in the Tarim Basin (Zhang et al., 2006). Extensive studies on the carbon isotopic record during the Ediacaran-Cambrian (E-C) transition suggested that the negative $\delta^{13}C$ anomaly occurred worldwide at the Precambrian-Cambrian boundary corresponded to the widespread development of an oxygen-deficient marine environment during transgression events (Kimura and Watanabe, 2001). Besides, some publications reported that the extreme negative $\delta^{13}C$ values most likely resulted from the oxidation of a large dissolved organic carbon pool in the deep ocean (Jiang et al., 2007; Och and Shields-Zhou, 2012; Ishikawa et al., 2013). During the early Cambrian, a transgressive event took place across the Tarim Basin. The episodic upwelling transported the ^{13}C-depleted basinal anoxic bottom seawater to the continental shelf, and then resulted in a regional negative ^{13}C anomaly in the Tarim Basin (Yao et al., 2014; Guo et al., 2017).

4.1.3. Stable carbon isotopic distribution of kerogens

The distribution of $\delta^{13}C_{Ker}$ values in the samples from the two studied sections is illustrated in Fig. 4. The carbon isotope ratios of 11 kerogens from the Yuertusi Formation ranged from −36.34‰ to −34.33‰ (average: −34.89‰). While the $\delta^{13}C_{Ker}$ values of the Xishanbulake and Xidashan Formations ranged from −34.64‰ to −31.59‰ (average: −32.65‰).

Some previous studies suggested that the composition of organic carbon isotopes is likely constrained from the original organism assemblages (Liu et al., 2016; Hu et al., 2018). For example, in the Tarim Basin the $\delta^{13}C_{Ker}$ values of the Lower Paleozoic source rocks dominated by benthic algae are usually smaller than −34‰, whereas those from the source rocks dominated by planktonic algae greater than −30‰ (Liu

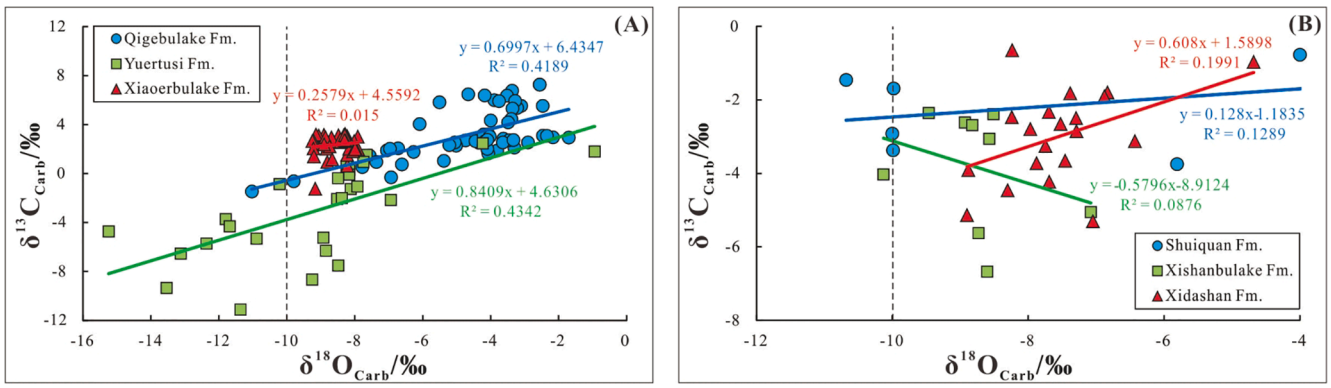

Fig. 2. Crossplots of $\delta^{13}C_{Carb}$-$\delta^{18}O_{Carb}$ for the (A) Shiairike and (B) Yaerdangshan sections.

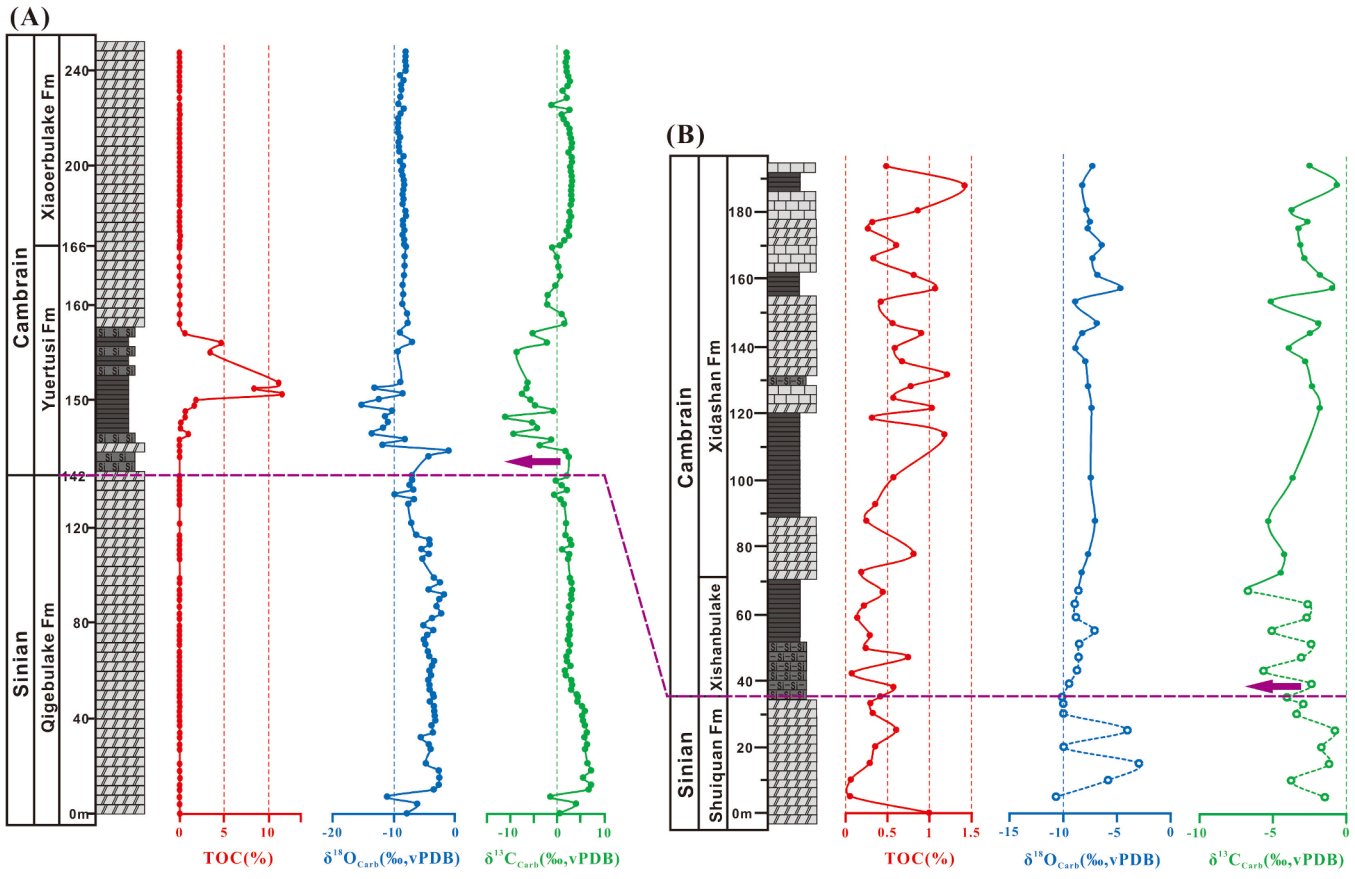

Fig. 3. TOC, $\delta^{13}C_{Carb,}$ and $\delta^{18}O_{Carb}$ profiles for the (A) Shiairike and (B) Yaerdangshan sections. The data represented by the hollow dots were chosen from the equivalent sequence of the northern Kuluketage area (Liu et al., 2017).

et al., 2016; Hu et al., 2018). Researchers have argued that species living at deep water with small growth rates have a much lower $\delta^{13}C$ value than faster-growing algae from the surface water (Wiencke and Fischer, 1990). Moreover, the high growth rate and small cell size of phytoplankton could result in a smaller degree of carbon isotope fractionation during photosynthesis (Laws et al., 1995; Close et al., 2011). Thus, the carbon isotopic ratio of the micro-planktonic algae is heavier than that of the macro-benthic algae.

A post-depositional alternation, such as bio- and/or thermal degradation, could also leave an influence on the $\delta^{13}C_{Ker}$ results. Considering the similar high thermal mature level of both Lower Cambrian strata studied in this work (Wang et al., 2003; Qiu et al., 2012; Yang et al., 2020), we inferred that different organism assemblages were responsible for the difference in $\delta^{13}C_{Ker}$ values between the Yuertusi Formation in the Shiairike and the Xishanbulake and Xidashan Formations in the Yaerdangshan section. So the Yuertusi Formation with $\delta^{13}C_{Ker}$ values smaller than −34‰ was dominated by benthic algae, while the Xishanbulake and Xidashan Formations dominated by benthic and planktonic algae. The Shiairike section was deposited at a shallow water with abundant sunlight conducive to the development of benthic algae compared to the deep water of the Yaerdangshan section. On the other hand, more input from the terrestrial detritus in the Kuluketage area (see the discussion in Section 4.1.4) would allow more planktonic algae to flourish. Therefore, there were different algae assemblages developed in the Shiairike and Yaerdangshan sections during the early Cambrian, which was supposed as the main reason for the different

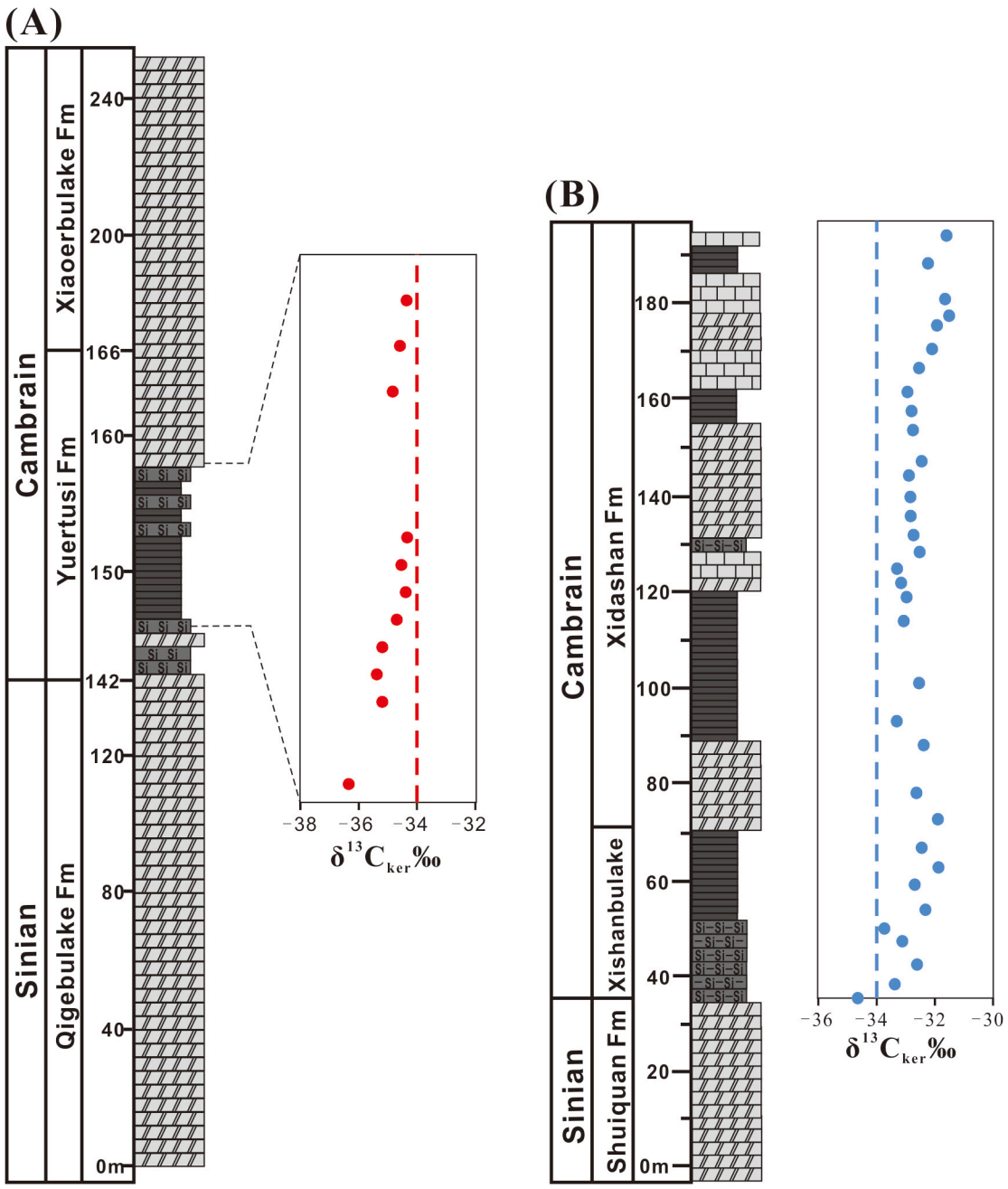

Fig. 4. The distribution profile of $\delta^{13}C_{Ker}$ in the (A) Yuertusi Formation and (B) Xishanbulake and Xidashan Formations (Data from Liu et al., 2017).

$\delta^{13}C_{Ker}$ results between these two sections.

4.1.4. Distribution of major and trace elements in the two sections

The distribution of trace element concentrations in the two sections is displayed in Fig. 5. Cherts and black shales of the Yuertusi Formation in the Shiairike section were extremely enriched in barium (Ba), cadmium (Cd), chromium (Cr), copper (Cu), molybdenum (Mo), nickel (Ni), phosphorus (P), vanadium (V), and zinc (Zn) (Fig. 5A), with varying concentrations of 126.5 to 10,000 ppm (average: 4476.89 ppm), 0.16 to 3.9 ppm (average: 1.4 ppm), 128 to 1384 ppm (average: 520.41 ppm), 28.8 to 129.5 ppm (average: 68.84 ppm), 1.11 to 39.5 ppm (average: 13.76 ppm), 30 to 65.6 ppm (average: 46.55 ppm), 60 to 5240 ppm (average: 1541.18 ppm), 31 to 1240 ppm (average: 344.15 ppm), and 8 to 244 ppm (average: 82.12 ppm), respectively. In the Yaerdangshan section, these elements were mostly concentrated in the Xishanbulake Formation (Fig. 5B), especially for the Ba (max. > 10,000 ppm), V (152 to 1935 ppm, average: 600.56 ppm), and Mo (18.2 to 79 ppm, average: 41.32 ppm). The average contents of Cd, Cu, Ni, and Zn in the Xishanbulake Formation from the northeastern part were either smaller than or similar to those in the Yuertusi Formation from the western part. However, the abundance of phosphorus was low in the Xishanbulake Formation varing from 120 to 790 ppm (average: 278 ppm).

During the E–C transition, the Tarim block evolved gradually from a rift basin to a passive continental margin basin (Turner 2010; Lin et al., 2012). Extensional tectonic movements along with large-scale volcanic and hydrothermal activities occurred during the E–C period (Yun et al., 2014; Zhou et al., 2014). For instance, volcanism was reported in the northeastern flank (Kuluketage) of the Tarim block (Jiang et al., 2000). Geochemical evidence of hydrothermal fluids was reported by some previous studies in the Lower Cambrian strata of the Tarim Basin (e.g., Sun et al., 2004; Yu et al., 2009; He et al., 2020). In such a tectonic-sedimentary setting, the extreme enrichment of Ba, Cd, Cu, Ni, V, and

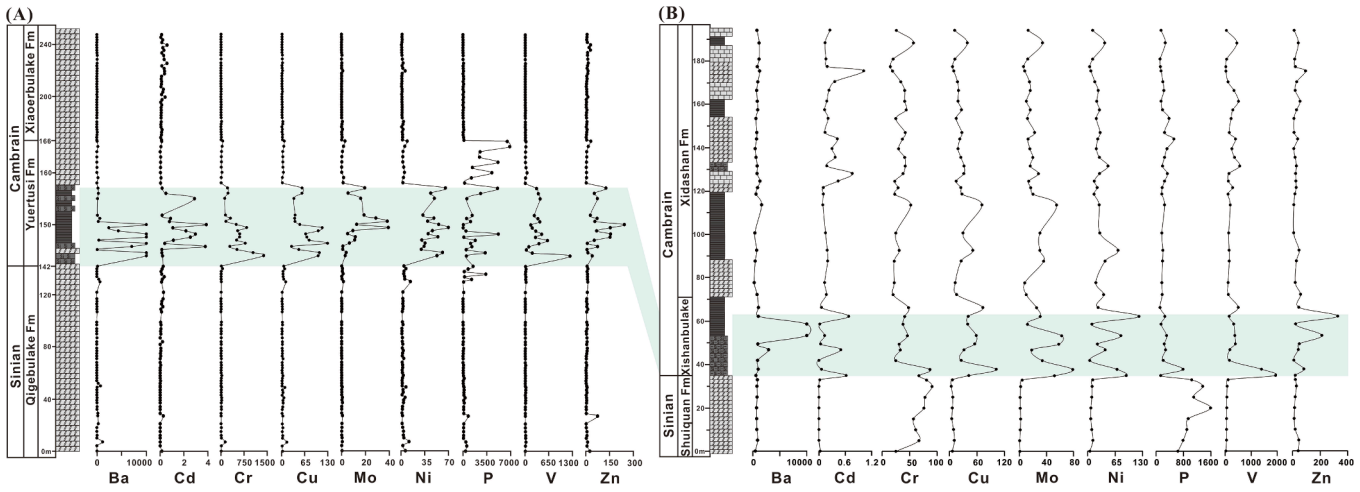

Fig. 5. Trace element profiles (ppm) in the (A) Shiairke and (B) Yaerdangshan sections.

Zn in the Lower Cambrian Yuertusi and Xishanbulake Formations is likely related to the widespread hydrothermal activities.

The Al/(Al + Mn + Fe) ratio can be applied to determine the origin of siliceous materials (Boström and Perterson, 1969; Adachi et al., 1986; Yamamoto, 1987). Typical hydrothermal deposits are characterized by Al/(Al + Mn + Fe) less than 0.6. In the Yuertusi Formation, the Al/(Al + Mn + Fe) ratios ranged from 0.07 to 0.62 reflecting a hydrothermal origin. This point was also strengthened in the Al-Fe-Mn ternary diagram for the Yuertusi Formation (Fig. 6A). However, neither the Al/(Al + Mn + Fe) ratios (ranging from 0.56 to 0.86) nor the Al-Fe-Mn diagram (Fig. 6B) for the Xishanbulake Formation demonstrated a hydrothermal event. This was probably due to a substantial continental debris input and a large sedimentation rate in the northeastern Tarim Basin.

The Al contents in sediment were predominantly sourced from aluminosilicate clay minerals and rarely affected by weathering or diagenesis, thereby providing a robust proxy for terrigenous flux assessment (Tribovillard et al., 2006; Calvert and Pedersen, 2007). The Al content in rocks from the Xishanbulake and Xidashan Formations (0.80–7.35%, average: 2.3%) was much larger than those from the Yuertusi Formation (0.06–2.33%, average: 0.58%), indicating more detritus input in the Xishanbulake and Xidashan Formations. This was also noticeable by the rather flat post-Archean Australia average shale (PAAS) normalized rare earth element (REE) patterns in the Xishanbulake Formation (Fig. 7B), which suggested a significant input of terrigenous detritus (Kamber and Webb, 2001; Nothdurft et al., 2004; Frimmel, 2009; Zhao et al., 2018). In contrast to the Xishanbulake Formation, the REE patterns of the Yuertusi Formation (Fig. 7A) were characterized by negative cerium (Ce) anomalies, negative europium (Eu) anomalies, and a slight depletion of light REEs, similar to the REE distribution patterns of seawater below the mixed layer (Elderfield and Greaves, 1982).

4.2. Depositional environment analysis

4.2.1. Evaluation of paleo-redox conditions

Trace elements are commonly utilized to infer the paleoenvironmental depositional conditions of sedimentary rocks (Algeo and Lyons, 2006; Algeo and Rowe, 2012; Tribovillard et al., 2006; Robbins et al., 2016). Redox-sensitive trace elements, such as Mo, U, V, etc., tend to be less soluble under reducing conditions, leading to their enrichment in oxygen-depleted sedimentary facies. This behavior allows their ratios and degree of enrichment in sedimentary rocks to serve as important representatives for paleo-redox conditions (Tribovillard et al., 2006). For example, U/Th > 1.25, V/(V + Ni) > 0.6, V/Cr > 4.25, and Ni/Co > 7 indicate anoxic conditions. These ratios tend to decrease with increasing oxidation level in the depositional environment (Jones and Manning, 1994; Kimura and Watanabe, 2001; Rimmer, 2004). The enrichment factor (EF) relative to PAAS was calculated by the equation $X_{EF} = (X/Al)_{sample}/(X/Al)_{PAAS}$ (Tribovillard et al., 2006), where X_{EF} represents the enrichment factor of element X, $(X/Al)_{sample}$ denotes the ratio of element X to Al in the sample, and $(X/Al)_{PAAS}$ stands for the ratio of element X to Al in PAAS. PAAS data for the normalization were taken from Taylor and McLennan (1985). EFs > 1 indicate an elemental enrichment relative to the PAAS concentrations; otherwise, they indicate a depletion of the elements.

A comprehensive description of paleo-redox conditions of the studied sections based on U/Th, V/(V + Ni), V/Cr, Ni/Co, and Mo_{EF}, U_{EF}, and V_{EF} is exhibited in Fig. 8. Although slight variations existed in the

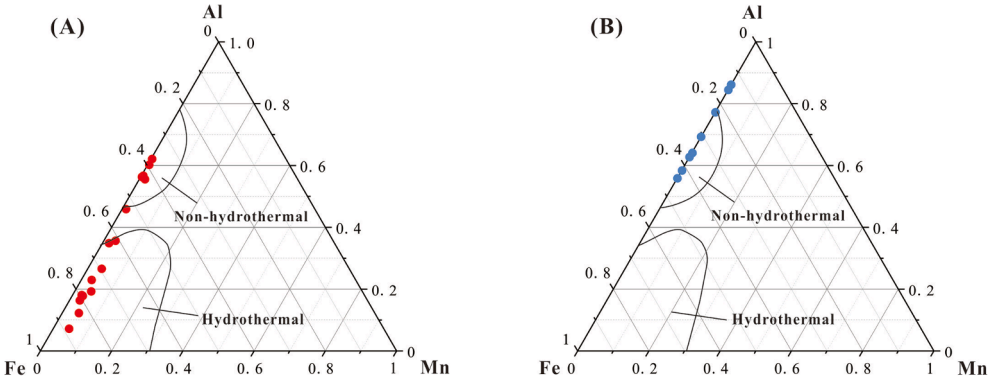

Fig. 6. Al-Fe-Mn ternary diagrams for the (A) Yuertusi and (B) Xishanbulake Formations.

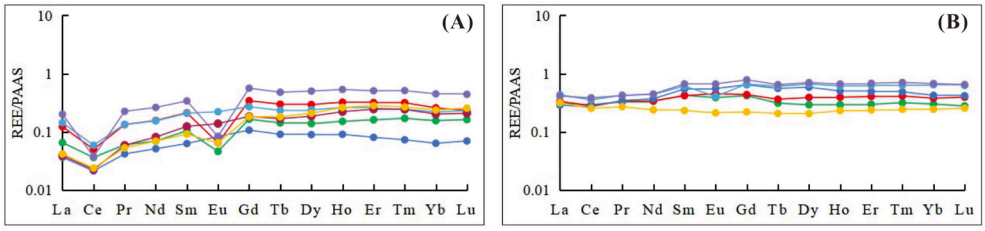

Fig. 7. PAAS-normalized REE patterns in cherts for the (A) Yuertusi and (B) Xishanbulake Formations.

absolute redox conditions based on the various proxies, the trend in all employed redox index indicated significant changes in the redox conditions. Generally, in the Shiairike section, dolostones of the Qigebulake, Xiaoerbulake, and the upper part of the Yuertusi Formations (TOC < 0.1%) were deposited in a suboxic-oxic condition. However, black shales and cherts from the lower part of the Yuertusi Formation extremely enriched in Mo, U, V (Mo_{EF}, U_{EF}, and V_{EF} > 100) and organic matter (maximum TOC content was 11.1%) were deposited in an anoxic settings. In the Yaerdangshan section, paleo-redox conditions in the ocean maintained an oxygen-deficiency state during the early Cambrian, accompanied by a TOC content less than 1.5%. The Xishanbulake and the lower part of the Xidashan Formation were deposited in anoxic conditions, while the upper part of the Xidashan Formation was deposited under suboxic-anoxic settings. These results indicated that the organic-rich rocks of the Lower Cambrian strata in the Tarim Basin were generally formed in a reducing environment.

4.2.2. Paleo-productivity appraisal

TOC, nutrient elements (e.g., P), and bioessential trace metals (e.g., Ba, Cu, Ni, and Zn) are good representatives for reconstructing paleo-productivity (Tribovillard et al., 2006; Calvert and Pedersen, 2007; Schoepfer et al., 2015). Organic carbon content provides the most direct representative for the paleo-productivity assessment (Shen et al., 2015). Phosphorus concentrations often showed a positive correlation with marine productivity. Its distribution in sediments or sedimentary rocks is often linked to the supply of organic matter. However, in an entirely reducing environment, there is a possibility of P sequestration from the sediment into the water column, leading to a low P concentration even in high productivity areas (Algeo and Ingall, 2007; Kraal, 2010). Ba, Cu, Ni, and Zn behave as micronutrients in biochemical cycles. They are usually delivered into the sediments along with organic matter sedimentation, and thus they are effective representatives for paleo-productivity. In the assessment of paleo-productivity with Ba, Cu, Ni, and Zn abundances, the detrital fraction should be estimated and subtracted. Al or Ti, typically detrital origin and immobile during diagenesis, are commonly used to estimate the detrital contribution (Tribovillard et al., 2006). The non-detrital fraction or the part above the average shale abundance (excess fraction) of Ba, Cu, Ni, and Zn should be calculated as follows: $X_{xs} = X_{total} - Ti \times (X/Ti)_{PAAS}$, where X_{xs}, X_{total}, Ti, and $(X/Ti)_{PAAS}$ represent the excess element X, the total X, titanium concentrations, and the ratio of element X to Ti in PAAS, respectively (Timothy and Calvert, 1998). Since no single representative is inherently more reliable than others, paleo-productivity assessments should be evaluated based on multiple representatives (Averyt and Paytan, 2004). Consequently, TOC, phosphorus concentration, Ba_{xs}, Cu_{xs}, Ni_{xs}, and Zn_{xs} were employed in this work to appraise the paleo-productivity variations in the Lower Cambrian strata in the Tarim Basin (Fig. 9).

In the Shiairike section, high concentrations of TOC (>10%), P (>1000 μg/g), Ba_{xs} (>1000 μg/g), Cu_{xs} (>1000 μg/g), and Zn_{xs} (>100 μg/g) were observed in the cherts and black shales of the Yuertusi Formation, indicating a high paleo-productivity. Abundant phosphorus was transported by the upwelling currents to the Yuertusi Formation (Zhang et al., 2007; Yu et al., 2009; Yang et al., 2014). In the Yaerdangshan section, the maximum values of Ba_{xs}, Cu_{xs}, Zn_{xs}, and Ni_{xs} were found in the Xishanbulake Formation, while the Xidashan Formation showed a moderate paleo-productivity. However, generally a low concentration of phosphorus less than 500 ppm in the Xishanbulake and Xidashan Formations might be due to the dilution from large quantities of terrigenous detritus.

4.3. Factors constraining the organic matter accumulation

Organic matter accumulation is generally controlled by multiple factors, including primary productivity, redox conditions, detritus influx, sedimentary rate, and hydrothermal activities (Pedersen and Calvert, 1990; Lanza-Espino and Soto, 1999; Sageman et al., 2003). Many studies have focused on the sedimentary lithofacies, paleogeography, and development model of the Lower Cambrian source rocks in the Tarim Basin. For instance, the thermal fluid activity, upwelling currents, and anoxic event model (Zhang et al., 2007) was developed for the craton marginal depression basin and platform-basin transition zone; and the gentle slope model was proposed developed in the middle-lower gentle slope and deep-water shelf facies belts, where source rocks formed (Pan et al., 2015; Chen et al., 2015; Tian et al., 2018). Zhu et al. (2016) modified the development model of the Yuertusi source rocks and proposed that they were developed in a middle-lower gentle slope sedimentary environment, controlled by multiple factors including upwelling, hydrothermal activity, sea-level eustacy and organic matter preservation conditions. Some other scholars believed that the organic-rich fine sediment of the Yuertusi Formation was deposited in an anoxic-suboxic restricted gulf lagoon environment, jointly controlled by high paleo-productivity and advantageous preservation conditions (Jin et al., 2020). Moreover, Zhang et al. (2020) suggested that the organic matter accumulation in the lower Yuertusi shale was controlled principally by high level of marine primary productivity and favorable conditions for organic matter preservation from a combination of silica-rich hydrothermal fluids and upwelling, while that in the upper shale might have been controlled predominantly by anoxic bottom water.

In this present study, high paleo-productivity and reducing conditions were found in both the Yuertusi and Xishanbulake Formations. Hence, the observed discrepancies in their TOC content might have originated from some other controlling factors, e.g. the different terrestrial detritus inputs and/or sedimentation rate, and distinguishing organism assemblages (Fig. 10).

The Yuertusi Formation in the Shiairike section of the western Tarim Basin was deposited in the middle-lower gentle slope and shallow shelf. A transgression, rapid regional rise in sea level occurred in the Tarim Basin during the early Cambrian. Phosphorus-rich upwelling and hydrothermal fluids brought plentiful nutrients (such as Ba, Cu, Ni, V, and Zn) having boosted the benthic algae. Providing that the benthic algae are more resistant to decomposition during the organic matter sedimentation, this can account for a higher TOC observed in the Yuertusi Formation compared with the Xishanbulake and Xidashan Formations, where more planktonic algae developed.

The Xishanbulake and Xidashan Formations in the Yaerdangshan section were deposited in an undercompensated deep water settings, with abundant nutrients from the volcanic and magmatic fluids, the primary biomass was dominated by planktonic algae, and their

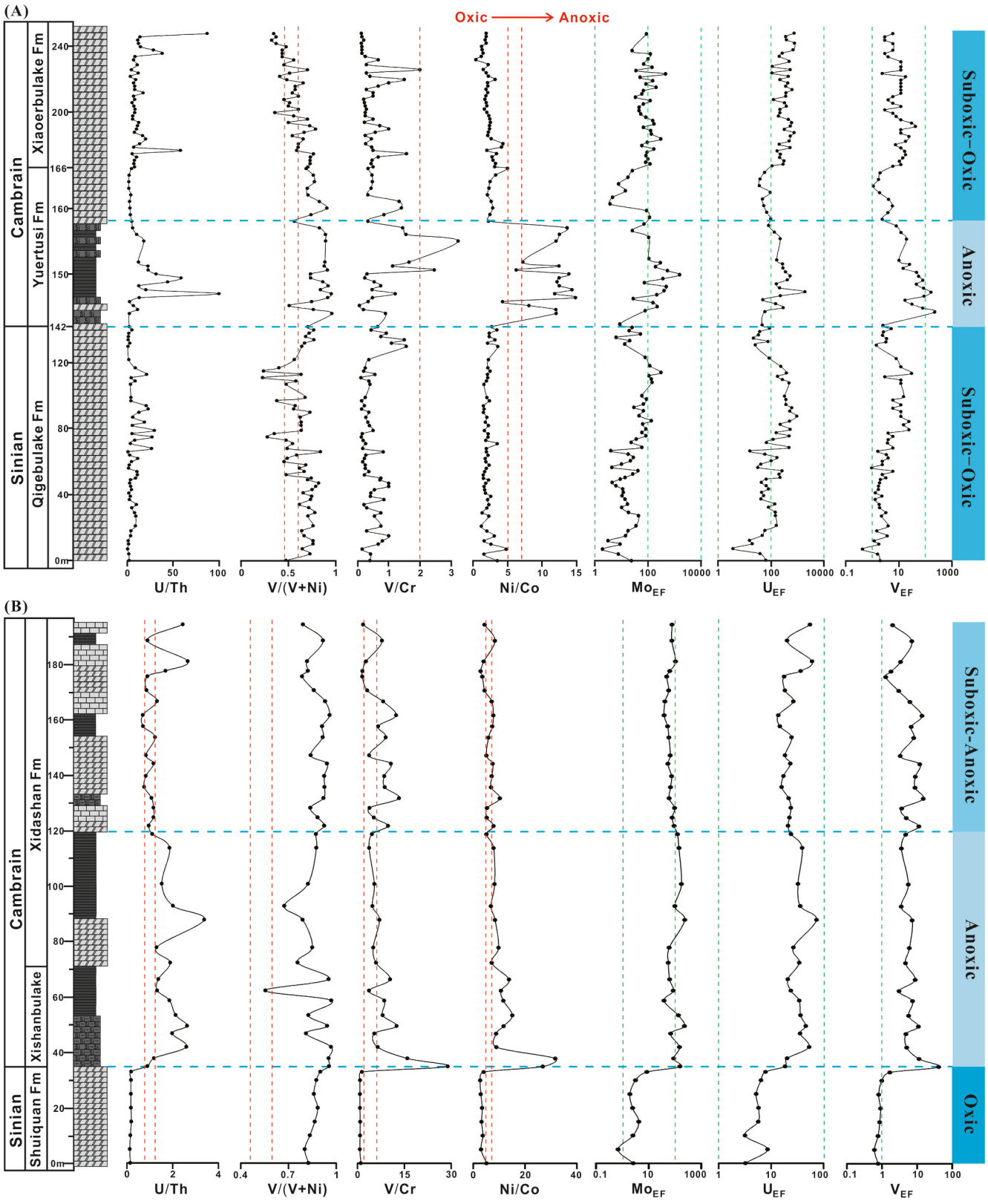

Fig. 8. Reconstruction of redox conditions for the (A) Shiairike and (B) Yaerdangshan sections.

remnants settled down to the anoxic seafloor as "sea snow" and incorporated into sediments. However, the high sedimentation rate and plenty detrital input might have diluted the organic matter flux into the sediments, resulting in a low TOC content of the Xishanbulake and Xidashan Formations compared to the western Yuertusi Formation.

5. Conclusions

In this study, the organic matter accumulation mechanisms of the Lower Cambrian successions in the western and northeastern margin of the Tarim Basin are discussed, particularly regarding the different

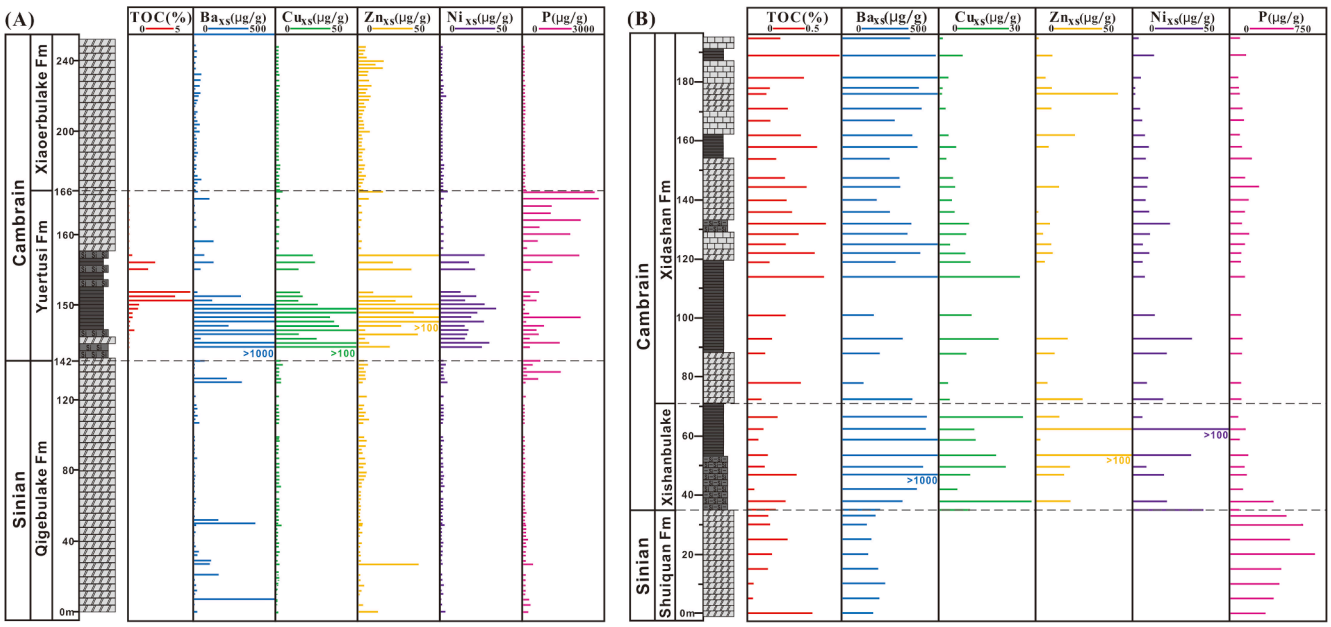

Fig. 9. Paleo-productivity profiles for the (A) Shiairike and (B) Yaerdangshan sections.

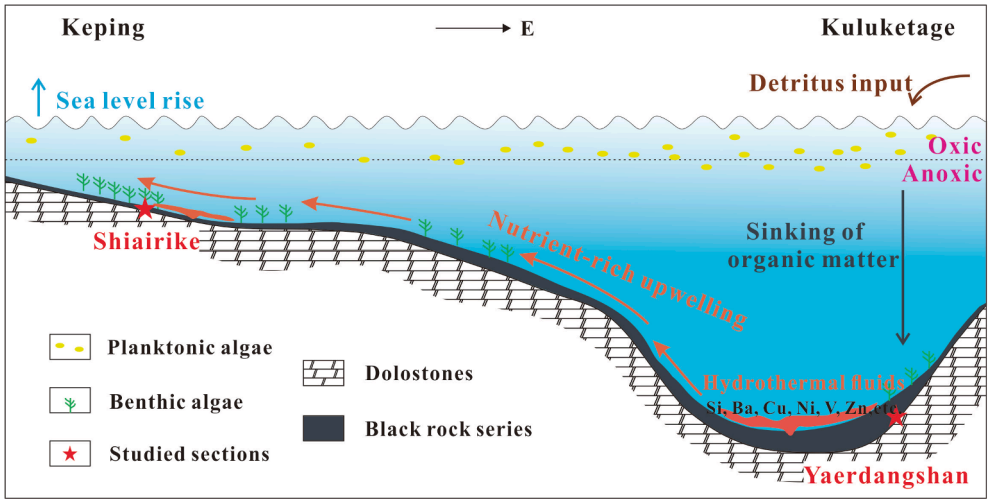

Fig. 10. The schematic model of the depositional environment for the Lower Cambrian strata in the western and northeastern margin of the Tarim Basin.

constraints of TOC accumulation in the two regions. By comparing geochemical records such as TOC, $\delta^{13}C_{Carb}$, $\delta^{13}C_{Ker}$, and major and trace elements in the sedimentary rocks of the Shiairike from the western and Yaerdangshan from the northeastern sections, the following conclusions were drawn:

(1) A negative $\delta^{13}C_{Carb}$ excursion at the base of the Cambrian in the Tarim Basin was observed, reflecting a widespread transgression event during the early Cambrian.
(2) Biomass development from different organism assemblages might have caused the distinguishing $\delta^{13}C_{Ker}$ results between the Yuertusi Formation and the Xishanbulake-Xidashan Formations, as the Yuertusi Formation was dominated by benthic algae while the Xishanbulake-Xidashan Formations dominated by a mixture of benthic and planktonic algae.
(3) Both the Yuertusi and Xishanbulake Formations were deposited in an anoxic environment, with high productivity enriched in Ba, Cu, Mo, Ni, V, and Zn from the active upwelling and hydrothermal fluids.
(4) Different organism assemblages and terrigenous detritus inputs might have brought about the different TOC content preserved in the Yuertusi Formation from western part and the Xishanbulake Formation from northeastern part. Higher biomass proportion from planktonic algae, more detritus input and faster sedimentation in the Xishanbulake Formation led to its lower TOC content in comparison to the Yuertusi Formation.

CRediT authorship contribution statement

Qian Deng: Conceptualization, Data curation, Formal analysis, Investigation, Visualization, Writing - original draft, Writing - review & editing. **Haozhe Wang:** Conceptualization, Formal analysis, Investigation. **Zhiwei Wei:** Conceptualization, Investigation. **Shida Li:** Conceptualization, Investigation. **Haizu Zhang:** Conceptualization, Resources. **Hu Liu:** Conceptualization, Data curation, Formal analysis. **Oluwabamise Lekan Faboya:** Conceptualization, Writing - review & editing. **Bin Cheng:** Conceptualization, Formal analysis. **Zewen Liao:** Conceptualization, Methodology, Funding acquisition, Supervision, Writing - review

& editing.

Declaration of Competing Interest

The authors declare that they have no known competing financial interests or personal relationships that could have appeared to influence the work reported in this paper.

Acknowledgments

This work was supported by the Strategic Priority Research Program of the Chinese Academy of Sciences (XDA14010103), the National Natural Science Foundation of China (42072145), and the National Oil and Gas Project of China (2017ZX05008002). We are very grateful to the editor and two anonymous reviewers for their constructive comments, which greatly helped to improve the original manuscript.

References

Adachi, M., Yamamoto, K., Sugisaki, R., 1986. Hydrothermal chert and associated siliceous rocks from the northern Pacific their geological significance as indication of ocean ridge activity. Sediment. Geol. 47, 125–148.
Algeo, T.J., Ingall, E., 2007. Sedimentary C_{org}: P ratios, paleocean ventilation, and Phanerozoic atmospheric pO_2. Palaeogeogr. Palaeoclimatol. Palaeoecol. 256, 130–155.
Algeo, T.J., Lyons, T.W., 2006. Mo–total organic carbon covariation in modern anoxic marine environments: implications for analysis of paleoredox and paleohydrographic conditions. Paleoceanography 21, 1–23.
Algeo, T.J., Rowe, H., 2012. Paleoceanographic applications of trace-metal concentration data. Chem. Geol. 324, 6–18.
Averyt, K.B., Paytan, A., 2004. A comparison of multiple proxies for export production in the equatorial Pacific. Paleoceanography 19, 4003–4016.
Boström, K., Perterson, M.N.A., 1969. The origin of aluminum-poor ferromanganoan sediments in areas of high heat-flow on the East Pacific Rise. Mar. Geol. 7, 427–447.
Calvert, S.E., Pedersen, T.F., 2007. Elemental proxies for paleoclimatic and palaeoceanographic variability in marine sediments: interpretation and application. Dev. Mar. Geol. 1, 567–644.
Chen, Q., Chu, C., Yang, X., Hu, G., Shi, Z., Jiang, H., Shen, B., Liu, W., 2015. Sedimentary model and development of the Cambrian source rocks in the Tarim Basin, NW China. Petrol. Geol. Exp. 37, 689–695 (in Chinese with English abstract).
Close, H.G., Bovee, R., Pearson, A., 2011. Inverse carbon isotope patterns of lipids and kerogen record heterogeneous primary biomass. Geobiology 9, 250–265.
Cohen, K.M., Finney, S.C., Gibbard, P.L., Fan, J.X., 2013. The ICS international chronostratigraphic chart. Episodes 36, 199–204.
Derry, L.A., 2010. A burial diagenesis origin for the Ediacaran Shuram-Wonoka carbon isotope anomaly. Earth Planet. Sci. Lett. 294, 152–162.
Dong, L., Xiao, S., Shen, B., Zhou, C., Li, G., Yao, J., 2009. Basal Cambrian microfossils from the Yangtze Gorges area (South China) and the Aksu area (Tarim block, northwestern China). J. Paleontol. 83, 30–44.
Elderfield, H., Greaves, M.J., 1982. The rare earth elements in seawater. Nature 296, 214–219.
Fang, X., Wu, L., Geng, A., Deng, Q., 2019. Formation and evolution of the Ediacaran to Lower Cambrian black shales in the Yangtze Platform, South China. Palaeogeogr. Palaeoclimatol. Palaeoecol. 527, 87–102.
Frimmel, H.E., 2009. Trace element distribution in Neoproterozoic carbonates as palaeoenvironmental indicator. Chem. Geol. 258, 338–353.
Fu, J., Qing, K., 1995. The Geochemistry of Kerogen. Guangdong Science and Technology Press, Guangzhou (in Chinese).
Guo, Q., Deng, Y., Hu, J., Wang, L., 2017. Carbonate carbon isotope evolution of seawater across the Ediacaran-Cambrian transition: evidence from the Keping area, Tarim Basin, NW China. Geol. Mag. 154, 1244–1256.
Han, T., Fan, H., Wen, H., 2018. Dwindling vanadium in seawater during the early Cambrian, South China. Chem. Geol. 492, 20–29.
He, D., Jia, C., Li, D., Zhang, C., Meng, Q., Shi, X., 2005. Formation and evolution of polycyclic superimposed Tarim Basin. Oil Gas Geol. 26, 64–77 (in Chinese with English abstract).
He, T., Lu, S., Li, W., Sun, D., Pan, W., Zhang, B., Tan, Z., Ying, J., 2020. Paleoweathering, hydrothermal activity and organic matter enrichment during the formation of earliest Cambrian black strata in the northwest Tarim Basin, China. J. Petrol. Sci. Eng. 189, 106987.
Hu, G., Meng, Q., Wang, J., Tengger, X.X., Lu, L., Liu, W., 2018. The original organism assemblages and kerogen carbon isotopic compositions of the early Paleozoic source rocks in the Tarim Basin, China. Acta Geol. Sin-Engl. 6, 2297–2309.
Ishikawa, T., Ueno, Y., Shu, D., Li, Y., Han, J., Guo, J., Yoshida, N., Komiya, T., 2013. Irreversible change of the oceanic carbon cycle in the earliest Cambrian: high resolution organic and inorganic carbon chemostratigraphy in the Three Gorges area, South China. Precambrian Res. 225, 190–208.
Jia, C., Wei, G., 2002. Tectonic characteristics and oil-bearing properties of the Tarim Basin. Chinese Sci. Bull. 47, 1–8 (in Chinese).
Jia, C., Zhang, S., Wu, S., 2004. Stratigraphy of the Tarim Basin and Adjacent Areas. Science Press, Beijing (in Chinese).
Jiang, C., Bai, K., Hei, A., Zhao, X., Zhang, X., Zhang, H., 2000. Petrology, geochemistry, magmatic process and source composition of Sinian-Cambrian volcanic rocks in Kuruktag area. Acta Petrol. Mineral. 19, 8–18 (in Chinese with English abstract).
Jiang, G., Kaufman, A.J., Christie-Blick, N., Zhang, S., Wu, H., 2007. Carbon isotope variability across the Ediacaran Yangtze platform in South China: Implications for a large surface-to-deep ocean $\delta^{13}C$ gradient. Earth Planet. Sci. Lett. 261, 303–320.
Jin, C., Li, C., Algeo, T.J., Planavsky, N.J., Cui, H., Yang, X., Zhao, Y., Zhang, X., Xie, S., 2016. A highly redox-heterogeneous ocean in South China during the early Cambrian (~529–514Ma): Implications for biota-environment co-evolution. Earth Planet. Sci. Lett. 441, 38–51.
Jin, Z., Tan, X., Tang, H., Shen, A., Qiao, Z., Zheng, J., Li, F., Zhang, S., Chen, L., Zhou, C., 2020. Sedimentary environment and petrological features of organic-rich fine sediments in shallow water overlapping deposits: a case study of Cambrian Yuertus Formation in northwestern Tarim Basin, NW China. Petrol. Explor. Dev. 47, 476–489 (in Chinese with English abstract).
Jones, B., Manning, D.A.C., 1994. Comparison of geochemical indices used for the interpretation of palaeoredox conditions in ancient mudstones. Chem. Geol. 111, 111–129.
Kamber, B.S., Webb, G.E., 2001. The geochemistry of late Archaean microbial carbonate: implications for ocean chemistry and continental erosion history. Geochim. Cosmochim. Acta 65, 2509–2525.
Kimura, H., Watanabe, Y., 2001. Oceanic anoxia at the Precambrian-Cambrian boundary. Geology 29, 995–998.
Kraal, P., 2010. Redox-dependent Phosphorus Burial in Modern and Ancient Marine Sediments (Ph.D. Dissertation). Universiteit Utrecht.
Lan, Z., Li, X., Chu, X., Tang, G., Yang, S., Yang, H., Liu, H., Jiang, T., Wang, T., 2017. SIMS U-Pb zircon ages and Ni-Mo-PGE geochemistry of the lower Cambrian Niutitang Formation in South China: constraints on Ni-Mo-PGE mineralization and stratigraphic correlations. J. Asian Earth Sci. 137, 141–162.
Lanza-Espino, G., Soto, L.A., 1999. Sedimentary geochemistry of hydrothermal vents in Guaymas Basin, Gulf of California, Mexico. Appl. Geochem. 14, 499–510.
Laws, E.A., Popp, B.N., Bidigare, R.R., Kennicutt, M.C., Macko, S.A., 1995. Dependence of phytoplankton carbon isotopic composition on growth rate and (CO_2) aq: theoretical considerations and experimental results. Geochim. Cosmochim. Acta 59, 1131–1138.
Li, M., Wu, G., Xia, B., Huang, T., Ni, B., Pang, S., Long, X., 2019. Controls on hydrocarbon accumulation in clastic reservoirs of the Tarim Craton, NW China. Mar. Petrol. Geol. 104, 423–437.
Li, X., Zhang, J., Wang, Y., Guo, M., Wang, Z., Wang, F., 2018. Accumulation condition and favorable area evaluation of shale gas from the Niutitang Formation in northern Guizhou, South China. J. Nat. Gas Geosci. 3, 1–10.
Lin, C., Li, H., Liu, J., 2012. Major unconformities, tectonostratigraphic framework, and evolution of the superimposed Tarim Basin, Northwest China. J. Earth Sci. 23, 395–407.
Liu, H., Liao, Z., Zhang, H., Tian, Y., Cheng, B., Yang, S., 2017. Stable isotope ($\delta^{13}C_{ker}$, $\delta^{13}C_{carb}$, $\delta^{18}O_{carb}$) distribution along a Cambrian outcrop section in the eastern Tarim Basin, NW China and its geochemical significance. Geosci. Front. 8, 163–170.
Liu, W., Hu, G., Tenger, Wang, J., Lu, L., Xie, X., 2016. Organism assemblages in the Paleozoic source rocks and their implications. Oil Gas Geol. 37, 617–626 (in Chinese with English abstract).
Liu, W., Zhang, G., Pan, W., Deng, S., Li, H., 2011. Lithofacies palaeogeography and sedimentary evolution of the Cambrian in Tarim area. J. Palaeogeogr. 13, 529–538 (in Chinese with English abstract).
Nothdurft, L.D., Webb, G.E., Kamber, B.S., 2004. Rare earth element geochemistry of Late Devonian reefal carbonates, Canning Basin, Western Australia: confirmation of a seawater REE proxy in ancient limestones. Geochim. Cosmochim. Acta 68, 263–283.
Och, L.M., Shields-Zhou, G.A., 2012. The Neoproterozoic oxygenation event: environmental perturbations and biogeochemical cycling. Earth Sci. Rev. 110, 26–57.
Pan, W., Chen, Y., Xiong, Y., Li, B., Xiong, R., 2015. Sedimentary facies research and implications to advantaged exploration regions on Lower Cambrian source rocks, Tarim Basin. Nat. Gas Geosci. 26, 1224–1232 (in Chinese with English abstract).
Pedersen, T.F., Calvert, S.E., 1990. Anoxia vs productivity: what controls the formation of organic-carbon-rich sediments and sedimentary rock? AAPG Bull. 74, 454–466.
Qian, Y., Feng, W., Li, G., Yang, A., Feng, M., Zhao, X., Xiao, B., 2009. Taxonomy and biostratigraphy of the Early Cambrian univalved mollusc fossils from Xinjiang. Acta Micropalaeontol. Sin. 26, 193–210 (in Chinese with English abstract).
Qiu, N., Chang, J., Zuo, Y., Wang, J., Li, H., 2012. Thermal evolution and maturation of lower Paleozoic source rocks in the Tarim Basin, northwest China. AAPG Bull. 96, 789–821.
Ren, R., Guan, S., Wu, L., Zhu, G., 2018. Evolution of the Neoproterozoic rift basins and its implication for oil and gas exploration in the Tarim Basin. Petrol. Res. 3, 66–76.
Rimmer, S.M., 2004. Geochemical Paleoredox Indicators in Devonian-Mississippian Black Shales, Central Appalachian Basin (USA). Chem. Geol. 206, 373–391.
Robbins, L.J., Lalonde, S.V., Planavsky, N.J., Partin, C.A., Reinhard, C.T., Kendall, B., Scott, C., Hardisty, D.S., Gill, B.C., Alessi, D.S., Dupont, C.L., Saito, M.A., Crowe, S. A., Poulton, S.W., Bekker, A., Lyons, T.W., Konhauser, K.O., 2016. Trace elements at the intersection of marine biological and geochemical evolution. Earth-Sci. Rev. 163, 323–348.
Sageman, B.B., Murphy, A.E., Werne, J.P., Ver Straeten, C.A., Hollander, D.J., Lyons, T. W., 2003. A tale of shales: the relative roles of production, decomposition, and dilution in the accumulation of organic-rich strata, Middle-Upper Devonian, Appalachian basin. Chem. Geol. 195, 229–273.

Schoepfer, S.D., Shen, J., Wei, H., Tyson, R.V., Ingall, E., Algeo, T.J., 2015. Total organic carbon, organic phosphorus, and biogenic barium fluxes as proxies for paleomarine productivity. Earth-Sci. Rev. 149, 23–52.
Shen, J., Schoepfer, S.D., Feng, Q., Zhou, L., Yu, J., Song, H., Wei, H., Algeo, T.J., 2015. Marine productivity changes during the end-Permian crisis and Early Triassic recovery. Earth-Sci. Rev. 149, 136–162.
Sun, X., Chen, J., Liu, W., Wang, D., 2004. Geochemical characteristics of cherts of Lower Cambrian in the Tarim Basin and its implication for environment. Petrol. Explor. Dev. 31, 45–48 (in Chinese with English abstract).
Taylor, S.R., McLennan, S.M., 1985. The Continental Crust: Its Composition and Evolution. Blackwell, Oxford.
Tian, L., Cui, H., Liu, J., Zhang, N., Shi, X., 2018. Early-Middle Cambrian paleogeography and depositional evolution of Tarim Basin. Oil Gas Geol. 39, 1011–1021 (in Chinese with English abstract).
Timothy, D.A., Calvert, S.E., 1998. Systematics of variations in excess Al and Al/Ti in sediment from the central equatorial Pacific. Paleoceanography 13, 127–130.
Tribovillard, N., Algeo, T.J., Lyons, T., Riboulleau, A., 2006. Trace metals as paleoredox and paleoproductivity proxies: an update. Chem. Geol. 232, 12–32.
Turner, S., 2010. Sedimentary record of Late Neoproterozoic rifting in the NW Tarim Basin, China. Precambrian Res. 181, 85–96.
Wan, Y., Zhang, S., Tang, S., Pan, Z., Wu, W., 2018. A comparative study of characterization of lower Palaeozoic Niutitang shale in northwestern Hunan, China. J. Nat. Gas Sci. Eng. 53, 284–300.
Wang, F., Zhang, S., Zhang, B., Xiao, Z., Liu, C., 2003. Maturity sand its history of Cambrian marine source rocks in the Tarim Basin. Geochimica 32, 461–468 (in Chinese with English abstract).
Wang, S., Zou, C., Dong, D., Wang, Y., Li, X., Huang, J., Guan, Q., 2015. Multiple controls on the Paleoenvironment of the early Cambrian marine black shales in the Sichuan Basin, SW China: Geochemical and organic carbon isotopic evidence. Mar. Petrol. Geol. 66, 660–672.
Wiencke, C., Fischer, G., 1990. Growth and stable carbon isotope composition of cold water macroalgae in relation to light and temperature. Mar. Ecol. Prog. Ser. 65, 283–292.
Yamamoto, K., 1987. Geochemical characteristics and depositional environments of cherts and associated rocks in the Franciscan and Shimanto Terranes. Sediment. Geol. 52, 65–108.
Yang, P., Wu, G., Ren, Z., Zhou, R., Zhao, J., Zhang, L., 2020. Tectono-thermal evolution of Cambrian-Ordovician source rocks and implications for hydrocarbon generation in the eastern Tarim basin, NW China. J. Asian Earth Sci. 194, 104267.
Yang, X., Li, H., Yong, Y., Liu, S., Li, J., Xiong, P., 2017. The strata and palaeo-geomorphology framework at the end of Neoproterozoic and development mode of source rocks at the beginning of Cambrian in Tarim Basin, China. J. Nat. Gas Geosci. 2, 313–322.
Yang, X., Xu, X., Chen, Q., Qian, Y., Chen, Y., Chu, C., 2014. Palaeotectonics pattern in Pre-Cambrian and its control on the deposition of the lower Cambrian source rocks in Tarim Basin, NW China. Nat. Gas Geosci. 25, 1164–1171 (in Chinese with English abstract).
Yao, C., Ma, D., Ding, H., Zhang, X., Huang, H., 2014. Trace elements and stable isotopic geochemistry of an Early Cambrian chert-phosphorite unit from the lower Yurtus Formation of the Sugetbrak section in the Tarim Basin. Sci. China: Earth Sci. 57, 454–464.
Yao, C., Guo, W., Liu, J., Li, H., 2017. Multiple proxies on the paleoenvironment of the Early Cambrian marine black rock series in the Tarim Basin, NW China: molybdenum isotope and trace element evidence. Int. J. Geosci. 8, 965–983.
Yao, J., Xiao, S., Yin, L., Li, G., Yuan, X., 2005. Basal Cambrian microfossils from the Yurtus and Xishanblaq formations (Tarim, Northwest China): systematic revision and biostratigraphic correlation of Micrhystridium-like acritarchs. Palaeontology 48, 687–708.
Yu, B., Dong, H., Widom, E., Chen, J., Lin, C., 2009. Geochemistry of basal Cambrian black shales and cherts from the Northern Tarim Basin, Northwest China: implications for depositional setting and tectonic history. J. Asian Earth Sci. 34, 418–436.
Yun, J., Jin, Z., Xie, G., 2014. Distribution of major hydrocarbon source rocks in the Lower Palaeozoic, Tarim Basin. Oil Gas Geol. 35, 827–838 (in Chinese with English abstract).
Zhang, B., Zhang, S., Bian, L., Jin, Z., Wang, D., 2007. Initial discussion on the developmental model of Neoproterozoic-Lower Paleozoic marine source rocks in South China. Sci. Bull. 52 (supplement I), 58–69 (in Chinese).
Zhang, C., Guan, S., Wu, L., Ren, R., Wang, L., Wu, X., 2020. Depositional environments of early Cambrian marine shale, northwestern Tarim Basin, China: implications for organic matter accumulation. J. Petrol. Sci. Eng. 194, 107497.
Zhang, C., Zou, H., Li, H., Wang, H., 2013. Tectonic framework and evolution of the Tarim Block in NW China. Gondwana Res. 23, 1306–1315.
Zhang, S., Wang, R., Jin, Z., Zhang, B., Wang, D., Bian, L., 2006. The relationship between the Cambrian-Ordovician high-TOC source rock development and paleoenvironment variations in the Tarim Basin, Western China: carbon and Oxygen isotope evidence. Acta Geol. Sin. 80, 459–466 (in Chinese with English abstract).
Zhang, S., Zhang, Y., Yan, H., 2015. Introduction to the stratigraphic chart of China (2014). J. Stratigr. 39, 359–366 (in Chinese with English abstract).
Zhang, Y., Yang, T., Hohl, S.V., Zhu, B., He, T., Pan, W., Chen, Y., Yao, X., Jiang, S., 2020. Seawater carbon and strontium isotope variations through the late Ediacaran to late Cambrian in the Tarim Basin. Precambrian Res. 345, 105769.
Zhao, J., Jin, Z., Hu, Q., Liu, K., Liu, G., Gao, B., Liu, Z., Zhang, Y., Wang, R., 2019. Geological controls on the accumulation of shale gas: a case study of the early Cambrian shale in the Upper Yangtze area. Mar. Petrol. Geol. 107, 423–437.
Zhao, Y., Zhao, M., Li, S., 2018. Evidences of hydrothermal fluids recorded in microfacies of the Ediacaran cap dolostone: geochemical implications in South China. Precambrian Res. 306, 1–21.
Zhou, X., Chen, D., Qing, H., Qian, Y., Wang, D., 2014. Submarine silica-rich hydrothermal activity during the earliest Cambrian in the Tarim Basin, northwest China. Int. Geol. Rev. 56, 1906–1918.
Zhu, G., Chen, F., Chen, Z., Zhang, Y., Xing, X., Tao, X., Ma, D., 2016. Discovery and basic characteristics of high-quality source rocks found in the Yuertusi Formation of the Cambrian in Tarim Basin, China. J. Nat. Gas Geosci. 1, 21–33.
Zhu, G., Zhang, Z., Zhou, X., Li, T., Han, J., Sun, C., 2019. The complexity, secondary geochemical process, genetic mechanism and distribution prediction of deep marine oil and gas in the Tarim Basin, China. Earth-Sci. Rev. 198, 102930.